Article

Discovery Medicine 2026; 38(209): 1824–1841
https://doi.org/10.24976/Discov.Med.202638209.142

Garcinol Protects Against Allergic Asthma by Suppressing Ferroptosis via the SIRT1/PPARα Signaling Pathway

Yanling Li[1], Feifei Feng[2], Yuezeng Zhao[2], Yanli Zhang[1], Boyi Xu[1], Qiao Zhang[2], Bin Luan[1,*]

[1]Department of Pediatric, Third Affiliated Hospital, Zhengzhou University, 450052 Zhengzhou, Henan, China
[2]College of Public Health, Zhengzhou University, 450001 Zhengzhou, Henan, China
*Correspondence: Luanbp117@163.com (Bin Luan)
Submitted: 28 January 2026 Revised: 9 May 2026 Accepted: 13 May 2026 Published: 20 June 2026

Background: Allergic asthma is a chronic inflammatory disorder of the airways, marked by airway hyperresponsiveness, overproduction of mucus, and structural alterations within the airway wall. Garcinol is a natural compound extracted from plants of the Garcinia genus and exhibits antitumor effects. This study aims to investigate the protective effects and underlying mechanisms of garcinol against asthma-induced lung injury in both *in vivo* and *in vitro* models, focusing on the role of ferroptosis.
Methods: An asthma mouse model was established by ovalbumin (OVA) sensitization, followed by treatment with garcinol or budesonide. Airway hyperresponsiveness was assessed, and bronchoalveolar lavage fluid (BALF) was collected for cell counts and inflammatory cytokine measurements. Lung tissues were harvested for histopathological staining. E-cadherin and Claudin-1 were examined using Western blot analysis to evaluate pathological alterations. Solute carrier family 7 member 11 (SLC7A11), ferroptosis suppressor protein 1 (FSP1), glutathione peroxidase 4 (GPX4), transferrin receptor 1 (TFR1), glutathione (GSH), malondialdehyde (MDA), iron content, and reactive oxygen species (ROS) levels were determined. Sirtuin 1 (SIRT1) and peroxisome proliferator–activated receptor alpha (PPARα) expression in lung tissues was analyzed. *In vitro*, human bronchial epithelial cells (BEAS-2B) were stimulated with interleukin-13 (IL-13) to establish a cellular asthma model and treated with garcinol, a ferroptosis inhibitor, or a SIRT1 inhibitor.
Results: Garcinol significantly alleviated airway hyperresponsiveness, attenuated the recruitment of inflammatory cells, and decreased cytokine concentrations in BALF. It attenuated lung tissue injury in the asthma mouse model. Garcinol markedly downregulated TFR1 expression while upregulating SLC7A11, GPX4, and FSP1. Garcinol decreased ROS and MDA levels and increased GSH content, thereby inhibiting ferroptosis. Garcinol also activated the SIRT1/PPARα signaling in lung tissues. *In vitro* experiments further confirmed that garcinol activated the SIRT1/PPARα pathway to regulate ferroptosis.
Conclusion: Garcinol exerts protective effects against allergic asthma–induced lung injury by activating the SIRT1/PPARα signaling pathway and suppressing ferroptosis.

Keywords: garcinol; asthma; lung injury; ferroptosis; sirtuin 1; peroxisome proliferator–activated receptor alpha

Introduction

Asthma is a prevalent long-term respiratory condition, impacting a vast global population numbering in the hundreds of millions [1]. Epidemiological data indicate that the global prevalence of asthma reaches 9.1% in children, 11.0% in adolescents, and 6.6% in adults, with a particularly high burden observed in low- and middle-income regions [2]. Beyond imposing substantial pressure on healthcare systems, the economic and social costs of asthma place a heavy burden on communities and individuals, posing a major public health challenge [1]. Pathologically, it involves sustained inflammation of the airways, increased airway hyperresponsiveness, and progressive structural changes within airway tissues [3,4]. Upon exposure to allergens or environmental pollutants, airway epithelial cells initiate a cascade of inflammatory responses by releasing cytokines and chemokines, which drive sustained airway inflammation [5]. In this process, T helper type 2 (Th2) immune responses play a central role and exacerbate inflammatory responses by secreting key cytokines such as interleukin (IL)-4, IL-5 and IL-13. Persistent airway inflammation then leads to airway remodeling and increased airway hyperresponsiveness, thereby aggravating asthma symptoms [6,7]. Airway remodeling is a hallmark of asthma progression and manifests as epithelial injury, basement membrane thickening, smooth muscle hyperplasia and hypertrophy, and abnormal extracellular matrix deposition [8,9]. Disruption of airway epithelial integrity is a key event underlying multiple pathophysiological alterations in asthma [10]. Currently, inhaled glucocorticoids remain the first-line therapy for asthma management. Although they effectively relieve acute symptoms, their long-term efficacy is often limited

due to persistent airway remodeling and chronic inflammation. Moreover, mechanisms associated with chronic inflammatory responses contribute to the development of drug resistance during long-term treatment [11]. Therefore, the development of novel therapeutic strategies, particularly those based on natural compounds, has become an important direction in asthma research.

Garcinol, a polyphenolic compound from the Garcinia genus, functions as a potent natural histone acetyltransferase (HAT) inhibitor and microRNA (miRNA) dysregulator [12,13]. Garcinol exhibits diverse biological activities, including immunomodulatory, antioxidant, anti-inflammatory, antitumor, and neuroprotective effects [14]. It has been shown to attenuate inflammation and oxidative stress in cerebral ischemia–reperfusion injury [15]. In addition, garcinol blocks reactive oxygen species (ROS) generation in Parkinson's disease models by activating the DJ-1/sirtuin-1 (SIRT1)-mediated antioxidant pathway [16]. In asthma research, garcinol has been reported to suppress asthma by inhibiting acetylation levels in lung $CD4^+$ T cells [17]. However, the precise mechanisms underlying the effects of garcinol on asthma remain unclear, and further investigation is therefore urgently needed.

Ferroptosis is a distinct form of regulated cell death driven by iron overload and the accumulation of lipid peroxidation products [18]. Unlike traditional forms of cell death, such as apoptosis, necrosis, or autophagy, ferroptosis is a form of regulated cell death caused by excessive iron accumulation and lipid peroxidation [19]. A study by Liu and colleagues [20] demonstrated that excessive iron ions may aggravate inflammatory responses and promote airway remodeling by activating the ferroptosis pathway. Recent studies have further suggested that the role of ferroptosis in asthma is primarily associated with oxidative stress responses and disturbances in iron metabolism, and its potential involvement in the progression of asthma has attracted increasing attention [21]. However, whether garcinol can regulate asthma by modulating ferroptosis has not yet been reported.

In this study, an experimental model of asthma was successfully induced in BALB/c mice through sensitization with ovalbumin (OVA), and garcinol was applied for *in vivo* intervention for the first time. Meanwhile, an IL-13-induced injury model was established in human bronchial epithelial cells (BEAS-2B), which were subsequently treated with garcinol. This study aimed to determine whether garcinol can attenuate asthma-induced lung injury and to investigate, using both mouse models and *in vitro* cellular models, whether garcinol regulates asthma through mechanisms involving ferroptosis. Ultimately, this study clarifies the protective effect of garcinol against asthma-induced lung injury and its key underlying mechanisms, providing experimental evidence and a theoretical basis for the potential application of garcinol in the treatment of allergic asthma.

Materials and Methods

Experimental Animals and Housing Conditions

Female BALB/c mice aged 6–8 weeks (body weight, 20 ± 2 g) were purchased from Henan Skbex Biotechnology Co., Ltd. (China). All animals were housed under specific pathogen-free conditions. The study protocol received approval from the Experimental Animal Ethics Committee of the Third Affiliated Hospital of Zhengzhou University (Approval No. 2024-097-01).

Establishment of the Murine Asthma Model and Grouping

After 1 week of acclimatization, fifty mice were randomly assigned to five groups (n = 10 per group): normal control group (CON), asthma model group (ovalbumin group, OVA), low-dose garcinol intervention group (OVA + LG), high-dose garcinol intervention group (OVA + HG), and budesonide intervention group (OVA + BUD).

An asthma model was established in all mice except those in the control group. Briefly, mice were sensitized by intraperitoneal injection of 0.2 mL sensitization solution (containing 100 µg OVA [HY-W250978, MedChemExpress, USA] and 1 mg aluminum hydroxide adjuvant) on days 1, 8, and 15 of the experiment. Following sensitization, beginning on day 21, mice were challenged with aerosolized 5% OVA for 30 min daily for 7 consecutive days using a self-constructed mouse nebulization chamber (30 cm × 25 cm × 30 cm) to establish the asthma mouse model [22]. In the garcinol intervention groups, the challenge phase was identical to that of the model group. During the sensitization phase, mice received intraperitoneal injections of garcinol (HY-107569, MedChemExpress, NJ, USA). The compound was administered at 10 mg/kg (low dose) or 20 mg/kg (high dose), 2 hours prior to nebulization. The treatment was administered for 14 consecutive days. The garcinol dosage was selected based on previously published studies [23]. Mice in the model control (OVA) group underwent the same sensitization and aerosol challenge procedures but received intraperitoneal injection of an equal volume of normal saline. Mice in the OVA + BUD group were nebulized with budesonide suspension (100 µg/kg, HJ20140475, AstraZeneca, Cambridge, UK) for 30 min, 30 min before each OVA challenge [24]. All mice were used for subsequent experiments 28 days after model establishment, and no mortality was observed during the experimental period.

Pulmonary Function Measurement

Twenty-four hours after the final intervention, mice were anesthetized by intraperitoneal injection of 50 mg/kg sodium pentobarbital (P3761, Sigma-Aldrich, MO, USA) and placed in the supine position on a surgical platform [22]. Pulmonary function was assessed using a small-animal lung function testing system (flexiVent, GYD Tech-

nology, Beijing, China). Mice were sequentially challenged with aerosolized acetyl-β-methylcholine chloride (methacholine, Mch) at concentrations of 0, 10, 25, and 100 mg/mL. Parameters, including airway resistance, tissue elastance and damping, were measured simultaneously. Before each dose escalation, residual solution in the nebulizer was thoroughly removed with sterile cotton swabs and rinsed three times with normal saline to prevent cross-contamination.

Collection of Bronchoalveolar Lavage Fluid (BALF)

After anesthesia with intraperitoneal sodium pentobarbital (50 mg/kg), the trachea and lungs were exposed under sterile conditions. Normal saline was slowly instilled through a tracheal cannula, followed by gentle chest massage for 20 s to ensure adequate alveolar lavage. BALF was collected into 1.5 mL Eppendorf tubes and centrifuged at 1000 *g* for 10 min at 4 °C. The supernatant was aliquoted and stored for subsequent analyses. The cell pellet was resuspended in 100 µL normal saline, and 20 µL of the suspension was smeared onto slides. Cells were stained with Wright–Giemsa stain and differential inflammatory cell counts were performed under a light microscope (BX53, Olympus Corporation, Tokyo, Japan).

Preparation and Collection of Lung Tissue Specimens

Mice in each group were euthanized 24 h after the final aerosol challenge by intraperitoneal injection of an overdose of sodium pentobarbital (150 mg/kg). After thoracotomy, the left lung was rapidly excised, ligated, placed into labeled cryovials, and immediately stored at –80 °C. Meanwhile, the right lung was perfused with 4% paraformaldehyde for *in situ* fixation, excised, and immersed in 4% formaldehyde for fixation in the dark for 48 h. After gradient alcohol dehydration, the tissues were sectioned into continuous 4-µm-thick sections for subsequent staining.

HE Staining

After fixation in 4% paraformaldehyde for 24 h, lung tissues were processed through a routine procedure including graded ethanol dehydration, xylene clearing, and paraffin embedding. Paraffin-embedded tissues were cut into 4-µm sections and mounted on glass slides. After deparaffinization in xylene and rehydration through graded ethanol, the sections were stained using a HE staining kit (G1120, Solarbio, Beijing, China). Briefly, sections were first stained with hematoxylin for 2–20 min, rinsed with running water, differentiated and blued, and subsequently stained with eosin for 30 s–2 min. After staining, the sections were dehydrated through graded ethanol, cleared with xylene, and mounted. Finally, the overall structure of lung tissue and inflammatory cell infiltration were observed under a light microscope (BX53, Olympus Corporation, Tokyo, Japan).

Masson Staining

Paraffin-embedded lung sections were first deparaffinized and rehydrated, then subjected to Masson's trichrome staining (G1340, Solarbio, Beijing, China) following the manufacturer's protocol. In brief, sections were stained with Ponceau–fuchsin for 5–10 minutes and rinsed in a weak acidic solution for 30 seconds. Differentiation was carried out using phosphomolybdic acid for 1–2 minutes, followed by another rinse in weak acid solution, and counterstaining with aniline blue for 1–2 minutes. Subsequently, sections were dehydrated through 95% and absolute ethanol, cleared in xylene, and mounted with neutral resin. Images were captured under a light microscope (BX53, Olympus Corporation, Tokyo, Japan), where collagen fibers appeared blue, while muscle fibers and cytoplasm appeared red, allowing assessment of the degree of pulmonary fibrosis.

Periodic Acid-Schiff (PAS) Staining

The paraffin sections of lung tissue were deparaffinized and rehydrated using a graded ethanol series and then stained according to the instructions of a PAS staining kit (G1008-20ML, Servicebio, Wuhan, China). Specifically, sections were first immersed in PAS reagent B for 10–15 min and rinsed with distilled water, followed by incubation with PAS reagent A at room temperature in the dark for 25–30 min. After rinsing with running water for 5 min, nuclei were counterstained with hematoxylin. Subsequently, sections were dehydrated with absolute ethanol, cleared in xylene, and mounted with neutral resin. Under a light microscope, PAS-positive substances appeared magenta, allowing evaluation of goblet cell hyperplasia and mucus secretion in the airway epithelium.

ROS Fluorescence Staining

Lung specimens were fixed in 4% paraformaldehyde for 24 hours before subsequent processing through a routine procedure, including graded ethanol dehydration, xylene clearing, and paraffin embedding. Frozen sections were ultimately prepared. Staining was performed according to the instructions of the ROS detection kit (DHE probe, HR9069, Bio-Lab, China). Briefly, tissue sections were first equilibrated to room temperature and washed with cleaning solution diluted in ultrapure water for 5 min. The sections were then incubated with the working solution containing the DHE probe at 37 °C for 30 min in the dark. After incubation, the sections were washed three times with phosphate-buffered saline (PBS, C0221A, Beyotime, Shanghai, China) to remove unbound probe, followed by nuclear counterstaining with DAPI (C1006, Beyotime, Shanghai, China) (incubated at room temperature in the dark for 10 min). After another PBS wash, the sections were mounted with an anti-fade mounting medium. Finally, images were captured under a fluorescence microscope (IX73, Olympus, Tokyo, Japan), and the intensity of red fluorescence reflected ROS levels in the tissue.

TUNEL Staining

TUNEL staining was performed on lung tissue sections using a TUNEL apoptosis detection kit (C1088, Beyotime Biotechnology) to evaluate cell apoptosis. Briefly, tissue sections were sequentially treated with xylene and a graded series of absolute ethanol. Once dried, the sections were digested with proteinase K solution at a concentration of 20 µg/mL and covered with buffer for incubation at room temperature for 12 min. The TUNEL reaction mixture (terminal deoxynucleotidyl transferase:fluorescent-labeled dUTP:reaction buffer = 1:5:50, v/v/v) was added to cover the tissue sections, which were then incubated in a 37 °C incubator for 1 h. DAPI solution (1 µg/mL) was applied for nuclear staining at room temperature in the dark for 10 min. The sections were mounted and observed under a fluorescence inverted microscope for image acquisition.

Prussian Blue Staining (DAB Enhancement)

To assess iron deposition in lung tissue, Prussian blue staining solution (DAB-enhanced) (R27072, Beyotime) was used. Briefly, lung tissues were fixed in 10% neutral formalin, followed by routine dehydration, paraffin embedding, and sectioning at a thickness of 4 µm. After deparaffinization and rehydration, sections were incubated with Perls' staining solution at room temperature for 20 min and rinsed with distilled water for 5 min. Subsequently, the DAB solution was applied for 5 min for color development, with the reaction monitored under a microscope. After termination, sections were washed with DAB buffer and distilled water. Hematoxylin counterstaining, differentiation, dehydration, clearing, and mounting were then performed. Finally, images were acquired under a light microscope, with iron deposition appearing as DAB-enhanced brownish-yellow signals.

Immunofluorescence Staining

Paraffin-embedded lung tissue sections (4 µm) were deparaffinized, rehydrated, and subjected to antigen retrieval using citrate buffer (pH 6.0). After cooling, sections were blocked with 5% BSA at room temperature for 30 min to reduce nonspecific binding. The sections were then incubated overnight at 4 °C with primary antibodies, including anti-SIRT1 antibody (1:200, ab110304, Abcam, UK) and anti-PPARα antibody (1:200, 15540-1-AP, Proteintech). The following day, sections were washed with PBS and incubated with the corresponding fluorescent-labeled secondary antibodies (Alexa Fluor 488 or Alexa Fluor 594, 1:500, Invitrogen) for 1 h in the dark. Nuclei were stained with DAPI for 5 min. Finally, the sections were mounted and observed under a fluorescence microscope (IX73, Olympus, Tokyo, Japan) for image acquisition.

Enzyme-Linked Immunosorbent Assay (ELISA)

Interleukin-4 (ml064310)/5 (ml063157)/13 (ml106729)/6 (ml063159)/1β (ml106733) in BALF were measured using kits obtained from Enzyme-linked Biotechnology (Shanghai, China). Mice serum or lung tissue homogenate supernatants were collected for the detection of inflammatory cytokine levels. Lung tissues were homogenized in pre-chilled PBS at a defined tissue-to-volume ratio, followed by centrifugation at 12,000 $\times$g for 10 min at 4 °C. The supernatants were then collected for subsequent analysis. The concentrations of inflammation-related cytokines were determined using the corresponding ELISA kits (Elabscience, Wuhan, China). All procedures were performed strictly according to the manufacturer's instructions. Briefly, standards and samples were added to antibody-precoated 96-well plates and incubated. After washing, the enzyme conjugate and chromogenic substrate were added sequentially. The reaction was terminated, and absorbance was measured at 450 nm using a microplate reader (Multiskan FC, Thermo Fisher Scientific, MA, USA).

Biochemical Assays

Oxidative stress-related biochemical indicators in lung tissue or serum were also measured using commercial kits. Lung tissues were homogenized in lysis buffer under ice-bath conditions and centrifuged at 4 °C. Biochemical assay kits (Jiancheng Bioengineering) were used to determine iron content (A039-2-1), glutathione (GSH; A006-1-1), and malondialdehyde (MDA; A003-4-1) levels in lung tissues and BEAS-2B cells, respectively. Absorbance values were measured using a microplate reader (Multiskan FC, Thermo Fisher Scientific, MA, USA) or spectrophotometer (Model UV-1800, Shimadzu, Kyoto, Japan) at the designated wavelengths. Final results were calculated according to the standard formulas and normalized to protein concentration or sample volume.

Western Blot Analysis (WB)

BEAS-2B cells and lung tissues were washed with phosphate-buffered saline (PBS) and lysed in RIPA buffer supplemented with a protease inhibitor cocktail, followed by incubation on ice for 30 min. Lysates were centrifuged at 12,000 $\times$g for 10 min at 4 °C, and supernatants were collected. Total protein concentration was determined using a bicinchoninic acid (BCA) protein assay kit (P0010S, Beyotime, Shanghai, China) according to the manufacturer's instructions. Protein samples were mixed with 5$\times$ sodium dodecyl sulfate (SDS) loading buffer at a ratio of 1:4 and denatured at 95 °C for 10 min. SDS–polyacrylamide gel electrophoresis (PAGE) gels were prepared in-house, and proteins were separated at 200 V for 30 min. Proteins were transferred onto polyvinylidene difluoride (PVDF) membranes at 400 mA for 25 min. Membranes were blocked with low-background rapid blocking

solution at room temperature for 20 min on a shaker (40 rpm) and then incubated with primary antibodies: anti-SIRT1 (1:1000; R25721, ZenBio, Chengdu, China), anti-PPAR (1:1000; 15540-1-AP; Proteintech), anti-SLC7A11 (1:1000; 32384-1-AP; Proteintech), anti-GPX4 (1:1000; 67763-1-Ig; Proteintech), anti-TFR1 (1:1000; 65236-1-Ig; Proteintech), anti-FSP1 (1:1000; 20886-1-AP; Proteintech), anti-E-cadherin (1:1000; 20874-1-AP; Proteintech), anti-Claudin-1 (1:1000; 13050-1-AP; Proteintech), and GAPDH (1:1000; 60004-1-Ig; Proteintech). After washing three times with TBST buffer, the membranes were incubated for 1 h at room temperature with horseradish peroxidase (HRP)-conjugated rabbit or mouse IgG secondary antibodies (ZB2301/ZB2305; Zhongshan Golden Bridge Biotechnology, Beijing, China). After removing excess liquid from the PVDF membrane with filter paper, the detection solution was evenly applied to the membrane surface, and signals were visualized using a chemiluminescence imaging system (Tanon 5200, Tanon Science & Technology, Shanghai, China). The ratio of the target protein to GAPDH was calculated for normalization. Subsequently, the normalized values for each treatment group were further standardized relative to the mean value of the control group, which was set to 1. The results for other groups were expressed as relative expression levels for statistical analysis and graphical presentation.

Cell Grouping

BEAS-2B cell (YC-B005, Yuanjing Biotechnology Co., Ltd., China) authentication was performed by a certified third-party service provider using short tandem repeat (STR) profiling, and the STR profile was confirmed to match the reference data in the DSMZ database. For mycoplasma contamination using PCR assay, no contamination was detected. Relevant authentication and mycoplasma testing reports are provided in the **Supplementary Materials**.

BEAS-2B cells were divided into eight groups, with each cellular experiment conducted in triplicate: (1) Control group: cells were cultured under standard conditions without any treatment; (2) IL-13 group: cells were treated with IL-13 at a concentration of 20 ng/mL for 48 h; (3) IL-13 + ferroptosis inhibitor group (IL-13 + Fer-1): cells were treated with 20 ng/mL IL-13 for 48 h, followed by incubation with complete medium containing 2 µM ferrostatin-1 (Fer-1, HY-100579, MedChemExpress, New Jersey, USA) for an additional 24 h [25]; (4) IL-13 + low-dose garcinol group (IL-13 + LG): cells were treated with 20 ng/mL IL-13 for 48 h and then exposed to 12.5 µM garcinol for 24 h; (5) IL-13 + high-dose garcinol group (IL-13 + HG): cells were treated with 20 ng/mL IL-13 for 48 h and then exposed to 25 µM garcinol for 24 h; (6) IL-13 + EX527 group: cells were treated with 20 ng/mL IL-13 for 48 h, followed by treatment with 15 µmol/L EX527 (SIRT1 inhibitor, HY-15452, MedChemExpress, New Jersey, USA) for 4 h [26]; (7) IL-13 + EX527 + low-dose garcinol group: cells were treated with 20 ng/mL IL-13 for 48 h, incubated with 15 µmol/L EX527 for 4 h, and subsequently treated with 12.5 µM garcinol for 24 h; (8) IL-13 + EX527 + high-dose garcinol group: cells were treated with 20 ng/mL IL-13 for 48 h, incubated with 15 µmol/L EX527 for 4 h, and subsequently treated with 25 µM garcinol for 24 h.

Cell Viability Assay

Cell viability of BEAS-2B cells under different treatment conditions was assessed using the Cell Counting Kit-8 (CCK-8) assay (C0042, Beyotime Biotechnology). Cells in the logarithmic growth phase were harvested and prepared as a single-cell suspension, then seeded into 96-well plates at a density of 8×10^3 cells per well (100 µL per well). The original medium was replaced with fresh culture medium containing the indicated treatments (three biological replicates per group). A blank control containing culture medium alone was also included. Cells were further cultured for 24 or 48 h. Subsequently, 10 µL of CCK-8 solution was added to each well, followed by an additional 2 h incubation. Absorbance was measured at 450 nm using a microplate reader, and cell viability was calculated using the following formula:

Cell viability (%) = (OD_sample – OD_blank) / (OD_control – OD_blank) × 100.

Statistical Analysis

All data are presented as mean ± standard deviation (Mean ± SD) and visualized using GraphPad Prism 8.0.2 (GraphPad Software, San Diego, CA, USA). Statistical analyses were performed using IBM SPSS Statistics 27 (IBM Corp., Armonk, NY, USA). The normality of the data was assessed using the Shapiro-Wilk test. Comparisons between two groups were conducted using an independent-samples *t*-test, with Welch's correction applied when variances were unequal. For comparisons among multiple groups, one-way or two-way ANOVA was used, followed by Tukey's post hoc test for pairwise group comparisons. A *p*-value of <0.05 was considered statistically significant.

Results

Effects of Garcinol on Lung Function and Inflammatory Indices in Asthmatic Mice

To determine the effects of garcinol on lung function and inflammatory parameters in asthmatic mice, an OVA-induced asthma mouse model was established. The results showed that, compared with the CON group, mice in the OVA group exhibited significantly increased airway resistance at different concentrations of methacholine (0, 10, 25, and 100 mg/mL) ($p < 0.05$, Fig. 1A). In addition, tissue elastance (H, Fig. 1B) and tissue damping (G, Fig. 1C) were both significantly increased in a dose-dependent manner ($p < 0.05$). Meanwhile, the total number of leukocytes,

eosinophils, and neutrophils, as well as the proportions of eosinophils and neutrophils in BALF, were markedly elevated ($p < 0.05$, Fig. 1D–H). The levels of inflammatory cytokines IL-4, IL-5, and IL-13 were also significantly increased ($p < 0.05$, Fig. 1I–K), indicating that OVA successfully induced airway hyperresponsiveness and pronounced airway inflammation. Compared with the OVA group, the garcinol low-dose group (OVA+LG), the garcinol high-dose group (OVA+HG), and the budesonide group (OVA+BUD) significantly reduced Rrs, H, and G in asthmatic mice ($p < 0.05$). Furthermore, the total leukocyte count and the infiltration of eosinophils and neutrophils in BALF were markedly decreased in all treatment groups, accompanied by significant reductions in IL-4, IL-5, and IL-13 levels ($p < 0.05$). These findings indicate that garcinol can reduce airway resistance, alleviate airway inflammation, and improve lung function, thereby exerting therapeutic effects against asthma, with efficacy comparable to budesonide.

Effects of Garcinol on Lung Histopathological Alterations in Asthmatic Mice

Lung tissues were subjected to HE, PAS, and Masson staining and examined under a light microscope (10 $\times$ 40). Compared with the CON group, the OVA group showed extensive peribronchial inflammatory cell infiltration, marked goblet cell hyperplasia, excessive collagen deposition, and pronounced airway lumen narrowing. In contrast, these pathological changes were markedly ameliorated in the OVA+LG, OVA+HG, and OVA+BUD groups (Fig. 2A–C). WB further demonstrated that protein levels of E-cadherin and Claudin-1 were significantly reduced in the OVA group, whereas their expression was significantly restored in the OVA+HG and OVA+BUD groups (Fig. 2D,E, $p < 0.05$). Collectively, these results suggest that garcinol, similar to BUD, alleviates airway inflammation, reduces goblet cell hyperplasia and collagen deposition, mitigates airway narrowing, and thereby attenuates asthma-related lung injury.

Effects of Garcinol on Ferroptosis in Lung Tissues of Asthmatic Mice

The percentage of TUNEL-positive cells in OVA-challenged mice was significantly increased. Garcinol and budesonide treatment markedly reduced TUNEL-positive rates dose-dependently (Fig. 3A,B), indicating that garcinol can attenuate cell death in asthmatic mouse lung tissue.

To determine whether cell death was associated with ferroptosis, oxidative stress in lung tissues was assessed using DHE fluorescent dye. OVA-challenged mice showed a markedly increased red fluorescent signal, indicating elevated ROS production ($p < 0.05$). In contrast, ROS-specific fluorescence intensity was significantly reduced in all intervention groups in a dose-dependent manner ($p < 0.05$, Fig. 3C,D). Confocal microscopy further confirmed colocalization of DAPI-stained nuclei (blue) with DHE-derived red signals, indicating substantial oxidative damage in the lungs of OVA-induced asthmatic mice.

Ferroptosis-related biological markers were further examined. Biochemical assays were used to measure iron content (Fig. 3E), GSH (Fig. 3F), and MDA (Fig. 3G) levels in lung tissues, while Western blotting assessed the expression of ferroptosis-regulatory proteins TFR1, SLC7A11, FSP1, and GPX4 (Fig. 3H). Compared with the CON group, OVA-challenged mice exhibited significantly decreased GSH levels and reduced expression of SLC7A11, FSP1, and GPX4, along with increased MDA levels, iron accumulation, and TFR1 expression. Treatment with garcinol (OVA+LG, OVA+HG) or budesonide (OVA+BUD) significantly reversed these changes ($p < 0.05$). Additionally, DAB-enhanced Prussian blue staining was used to assess iron deposition in lung tissues. OVA-challenged mice showed pronounced iron overload, which was effectively alleviated following intervention ($p < 0.05$, Fig. 3I). Collectively, these changes in multiple ferroptosis-related markers suggest that garcinol alleviates OVA-induced oxidative damage and ferroptosis in lung tissue by regulating iron homeostasis and antioxidant systems.

Effects of Garcinol on SIRT1 and PPARα Expression

Immunofluorescence histochemistry (Fig. 4A,B) and Western blotting (Fig. 4C,D) were used to evaluate SIRT1 and PPARα expression in lung tissues from each group. Nuclei were counterstained with DAPI, exhibiting blue fluorescence under UV excitation, while SIRT1 and PPARα were specifically labeled via green and red fluorescence channels, respectively. OVA-challenged mice exhibited reduced mean fluorescence intensity and SIRT1 and PPARα protein levels ($p < 0.05$). Treatment with garcinol (OVA+LG, OVA+HG) or budesonide (OVA+BUD) significantly increased the mean fluorescence intensity and protein expression of these two proteins.

Effects of Garcinol on IL-13–Induced BEAS-2B Cells

An *in vitro* asthma model was established using IL-13–treated BEAS-2B cells. IL-13 at concentrations $\geq$20 ng/mL significantly reduced cell viability (Fig. 5A) and markedly increased secretion of IL-6 and IL-1β (Fig. 5B,C), indicating robust inflammatory activation. Garcinol at concentrations $\leq$25 μM exhibited no obvious cytotoxicity (Fig. 5D) and dose-dependently suppressed IL-13–induced IL-6 and IL-1β secretion (Fig. 5E,F). WB analysis showed that IL-13 significantly downregulated Claudin-1 and E-cadherin expression (Fig. 5G,H) and reduced SIRT1 and PPARα levels (Fig. 5I,J), whereas garcinol treatment markedly reversed these changes. In addition, IL-13 induced ferroptosis-related alterations characterized by increased TFR1 expression and decreased SLC7A11, GPX4, and FSP1 expression, all of which were significantly reversed by garcinol treatment (Fig. 5K). These findings in-

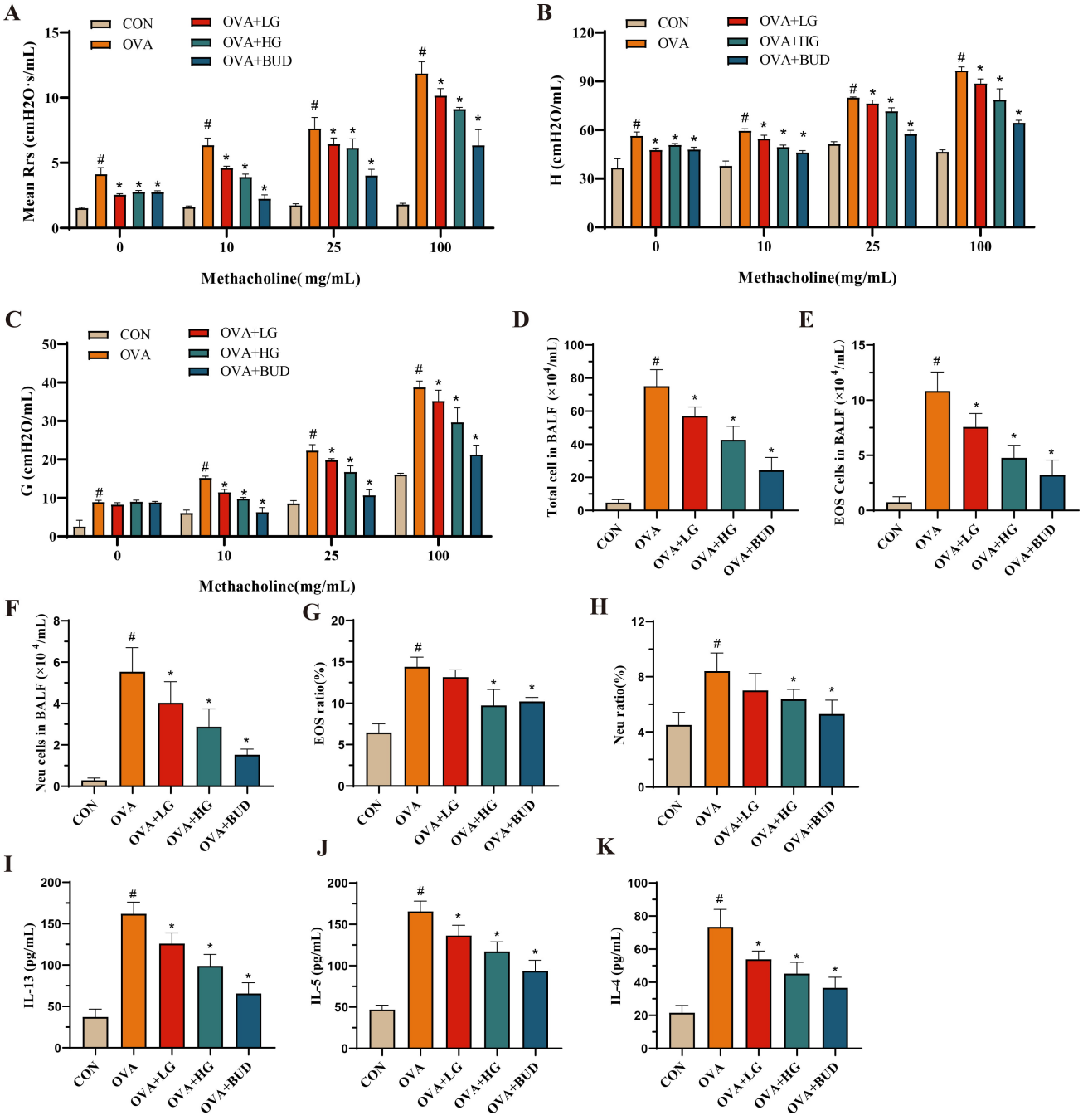

Fig. 1. Effects of garcinol on lung function and airway inflammation in OVA-induced asthmatic mice. (A–C) Airway resistance (Rrs), tissue damping (G), and tissue elastance (H) in mice from each group. (D–H) Total leukocyte count (D), and the numbers and percentages of eosinophils (E,G) and neutrophils (F,H) in BALF. (I–K) ELISA analysis of IL-13 (I), IL-5 (J), and IL-4 (K) levels in BALF from each group. N = 10, $^{\#}p < 0.05$ vs. CON group. $^{*}p < 0.05$ vs. OVA group. OVA, ovalbumin; BALF, bronchoalveolar lavage fluid; ELISA, Enzyme-Linked Immunosorbent Assay; IL, interleukin; CON, control.

dicate that garcinol alleviates IL-13–induced BEAS-2B cell injury by suppressing inflammation, preserving epithelial barrier integrity, and modulating ferroptosis-related pathways.

Ferroptosis Inhibition on IL-13–Treated BEAS-2B Cells

BEAS-2B cells cultured with IL-13 were treated with Ferrostatin-1 (Fer-1), a specific ferroptosis inhibitor, to investigate the role of ferroptosis in airway epithelial barrier injury. The expression levels of epithelial barrier proteins (E-cadherin, Claudin-1; Fig. 6A,B) and

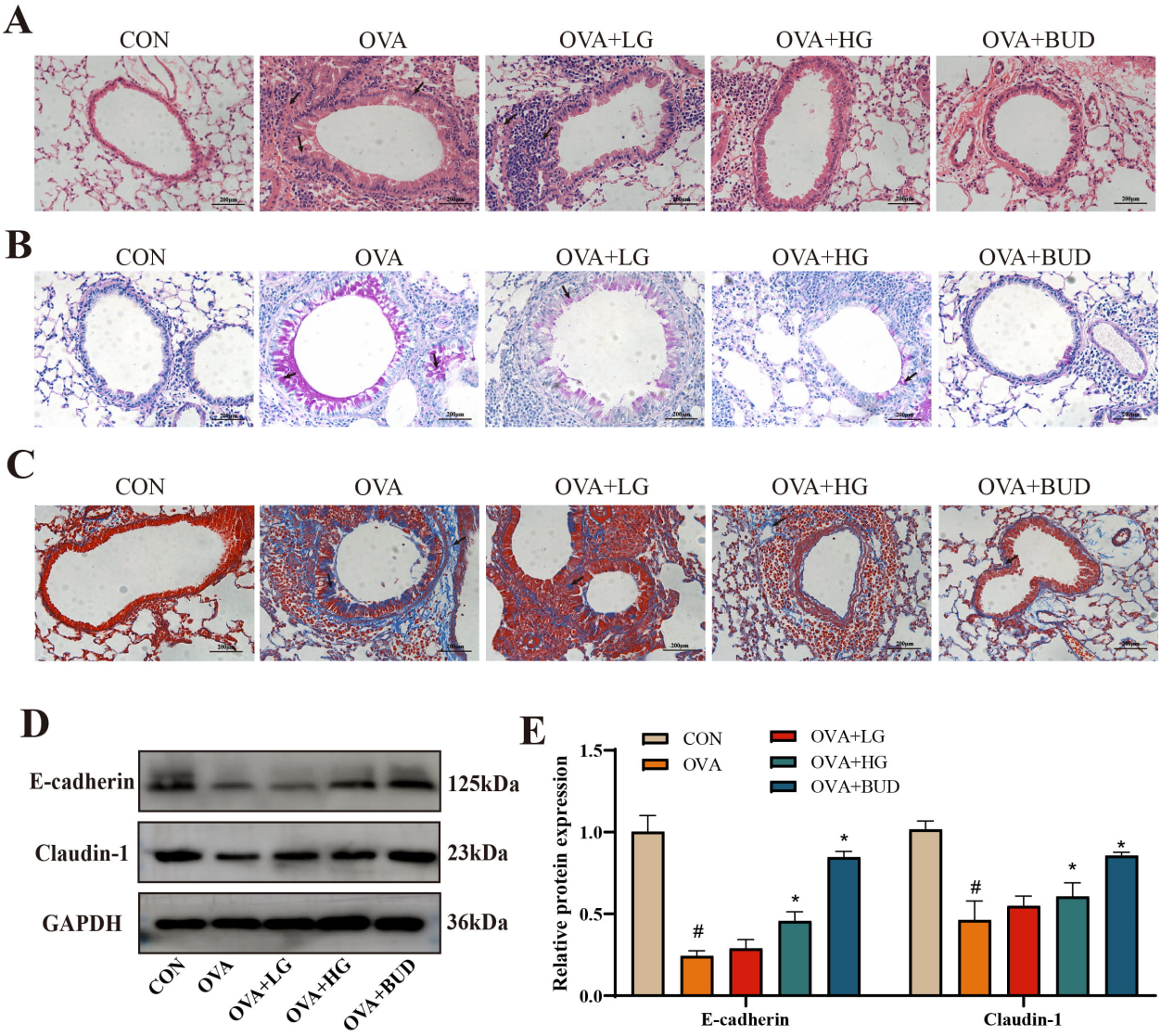

Fig. 2. Effects of garcinol on lung histopathology and E-cadherin and Claudin-1 protein expression in asthmatic mice. (A) HE staining of lung tissues from each group, with arrows indicating inflammatory cell infiltration and exudation; scale bar = 200 µm. (B) PAS staining of lung tissues, arrows indicate overproduced mucus and goblet cells; scale bar = 200 µm. (C) Masson's trichrome staining of lung tissues, arrows indicate collagen fiber deposition; scale bar = 200 µm. (D,E) WB analysis of E-cadherin and Claudin-1 expression in lung tissues from each group (n = 3). $^{\#}p < 0.05$ vs. CON group. $^{*}p < 0.05$ vs. OVA group. HE, Hematoxylin and Eosin; PAS, Periodic acid-Schiff; WB, Western blot.

key ferroptosis-related proteins (SLC7A11, FSP1, GPX4, TFR1; Fig. 6C,D) were assessed by WB. IL-13 stimulation significantly downregulated the protein levels of E-cadherin, Claudin-1, SLC7A11, FSP1, and GPX4 ($p < 0.05$), while significantly upregulating TFR1 expression ($p < 0.05$). Conversely, co-treatment with Fer-1 significantly reversed these alterations, increasing the levels of E-cadherin, Claudin-1, SLC7A11, FSP1, and GPX4, and decreasing TFR1 expression ($p < 0.05$). These results indicate that inhibiting ferroptosis effectively mitigates IL-13-induced ferroptosis and alleviates damage to the airway epithelial barrier. These findings align with the *in vivo* results.

Effects of Garcinol on IL-13–Treated BEAS-2B Cells After SIRT1 Inhibition by EX527

Cell viability of IL-13-stimulated BEAS-2B cells under different concentrations of EX527 (a SIRT1 inhibitor) was measured using the CCK-8 assay. IL-13 stimulation significantly reduced cell viability ($p < 0.05$). Cell viability showed a concentration-dependent decrease with increasing EX527 concentration. A statistically significant reduction was observed at 15 µmol/L EX527 ($p < 0.05$, Fig. 7A). Therefore, 15 µmol/L EX527 was selected as the optimal concentration for subsequent experiments.

WB was performed to assess the expression levels of SIRT1 and PPARα proteins (Fig. 7B,C). IL-13 stimulation

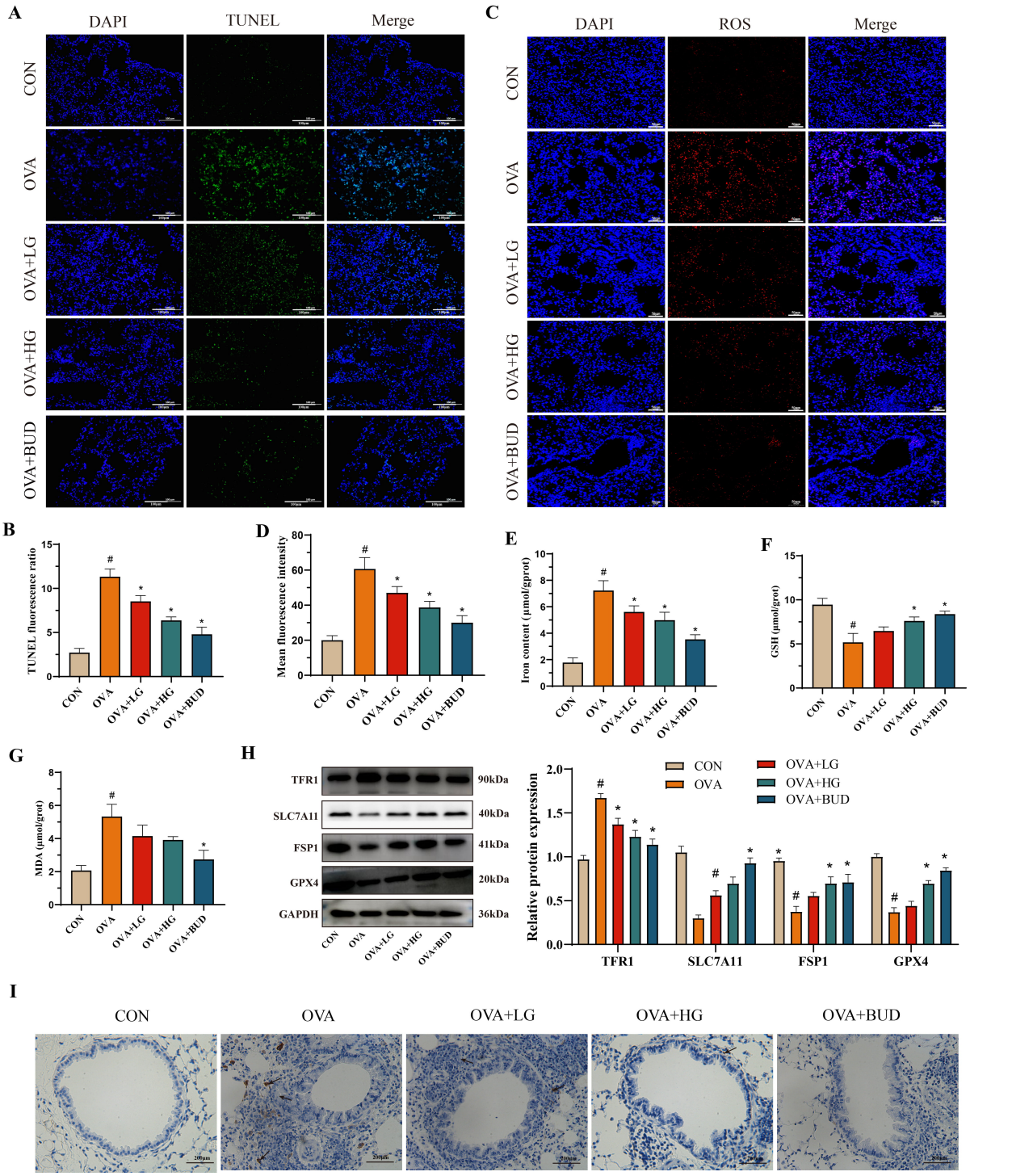

Fig. 3. Effects of garcinol on ferroptosis. (A) TUNEL staining of lung tissues from each group. Nuclei were counterstained with DAPI, showing blue fluorescence under UV excitation, while FITC-labeled TUNEL-positive cells exhibited characteristic green fluorescence (scale bar = 100 μm). (B) TUNEL-positive cell ratio. (C) ROS fluorescence staining (DHE fluorescence) of lung tissues from each group (scale bar = 50 μm). (D) Average ROS fluorescence intensity in lung tissues from each group. (E–G) Biochemical assays measuring iron content (E), GSH levels (F), and MDA levels (G). (H) Western blot analysis of ferroptosis-related proteins TFR1, SLC7A11, FSP1, and GPX4 in lung tissues. (I) Prussian blue staining of lung tissues (DAB-enhanced, ×200) with arrows indicating iron deposition, showing brown coloration. N = 10, $^{\#}p < 0.05$ vs. CON group. $^{*}p < 0.05$ vs. OVA group. TUNEL, Terminal deoxynucleotidyl transferase dUTP nick end labeling; DAPI, 4',6-diamidino-2-phenylindole; UV, Ultraviolet; FITC, Fluorescein isothiocyanate; ROS, reactive oxygen species; GSH, glutathione; MDA, malondialdehyde; TFR1, transferrin receptor 1; SLC7A11, Solute carrier family 7 member 11; FSP1, ferroptosis suppressor protein 1; GPX4, glutathione peroxidase 4; DAB, 3,3'-Diaminobenzidine.

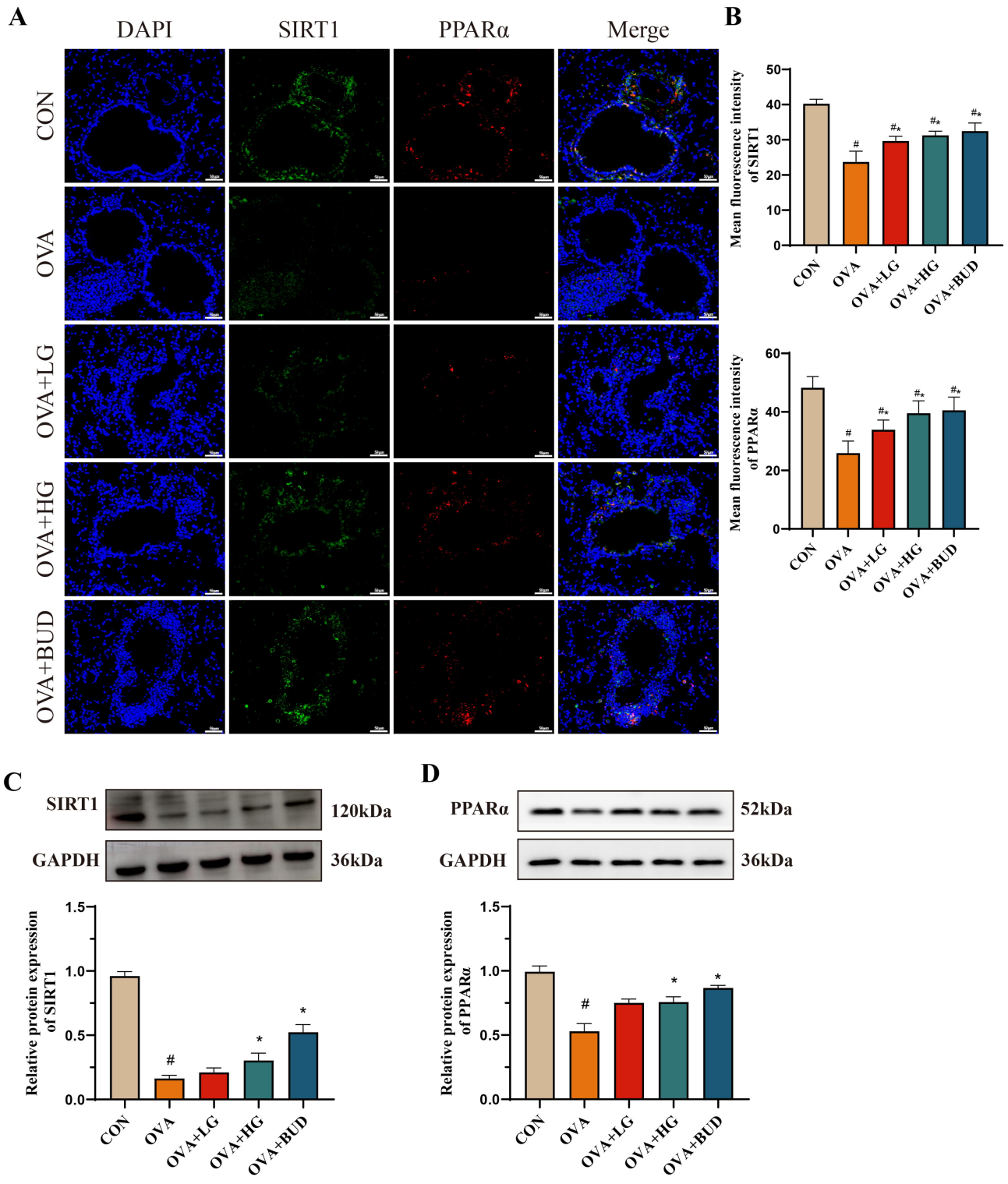

Fig. 4. Garcinol on SIRT1 and PPARα expression. (A,B) Immunofluorescence staining and quantitative analysis of SIRT1 and PPARα expression; scale bar = 50 µm. (C,D) Western blot analysis and quantitative densitometry of SIRT1 and PPARα protein levels in lung tissues from each group. N = 10, $^{\#}p < 0.05$ vs. CON group. $^{*}p < 0.05$ vs. OVA group. SIRT1, Sirtuin 1; PPARα, peroxisome proliferator–activated receptor alpha.

significantly decreased the expression of both SIRT1 and PPARα compared to the control ($p < 0.05$). Treatment with garcinol significantly increased the levels of SIRT1 and PPARα proteins ($p < 0.05$), suggesting its regulatory effect on the SIRT1/PPARα pathway. In contrast, co-treatment with the SIRT1 inhibitor EX527 significantly re-

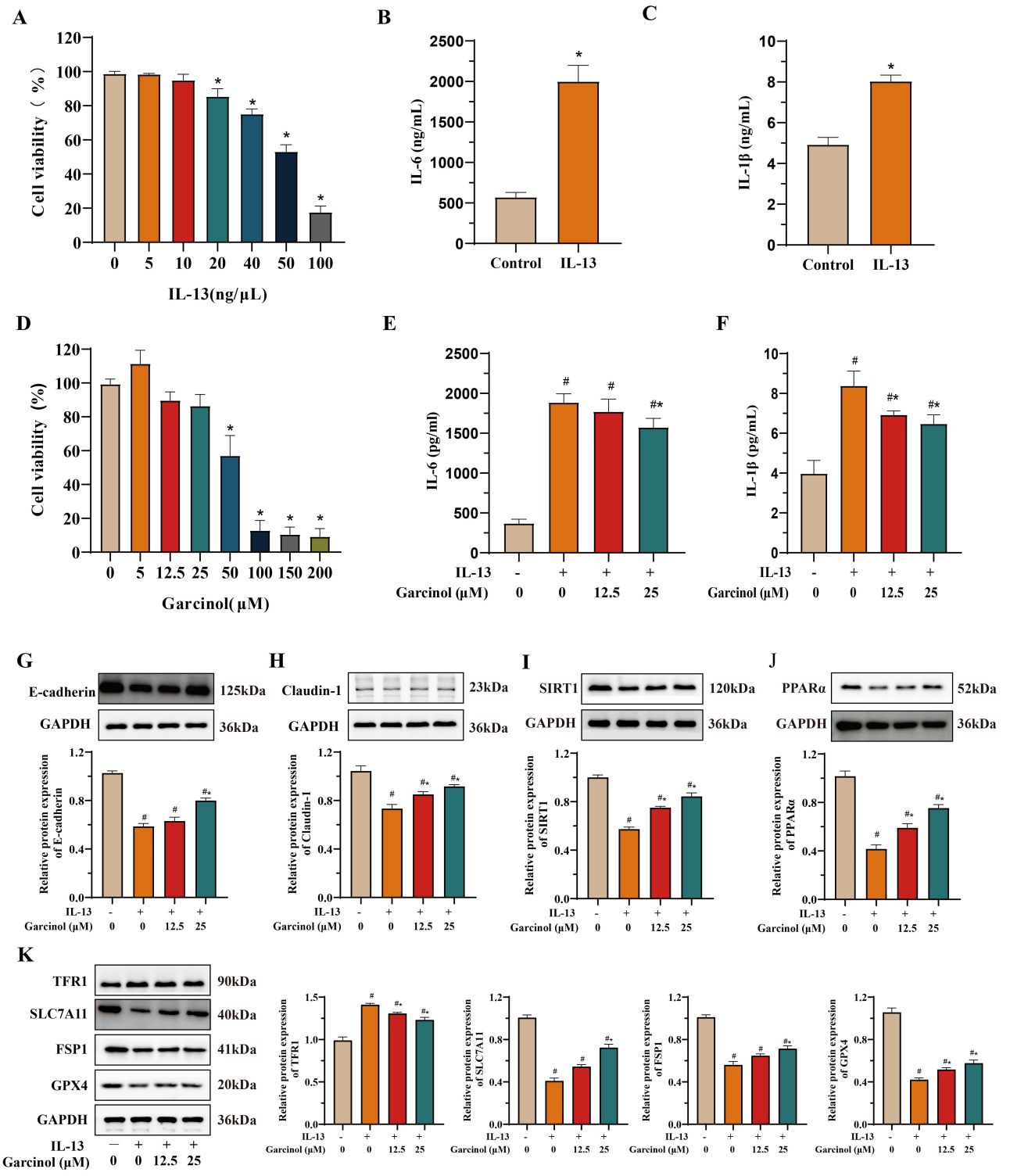

Fig. 5. Effects of garcinol on IL-13–induced inflammatory response, barrier dysfunction, and ferroptosis-related changes in BEAS-2B. (A,D) CCK-8 assay. (B,C,E,F) ELISA measurement of IL-6 and IL-1β secretion levels in cell culture supernatants. (G–J) Western blot analysis of airway epithelial barrier proteins (E-cadherin, Claudin-1) and SIRT1/PPARα-related proteins. (K) Western blot analysis of ferroptosis-related protein expression. N = 10, $^{\#}p < 0.05$ vs. Control group; $^{*}p < 0.05$ vs. IL-13 group. BEAS-2B, human bronchial epithelial cells; CCK-8, Cell Counting Kit-8.

duced SIRT1 and PPARα expression, indicating that garcinol's effect may involve the activation of the SIRT1/PPARα signaling axis in IL-13-stimulated BEAS-2B cells.

Intracellular levels of GSH, MDA, and iron content were measured using biochemical assay kits (Fig. 7D–F), while the expression of ferroptosis-related proteins (TFR1,

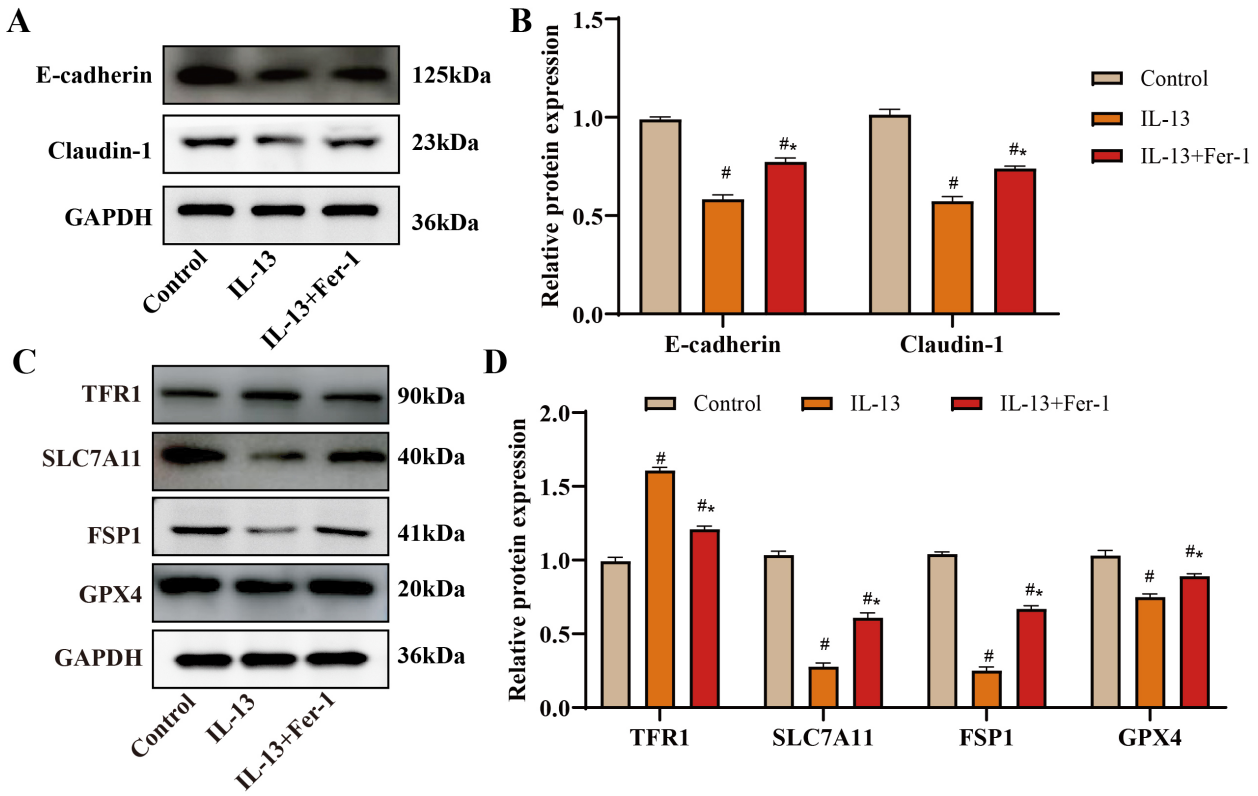

Fig. 6. Effects of ferroptosis inhibition on E-cadherin, Claudin-1, SLC7A11, FSP1, GPX4, and TFR1 protein expression in IL-13–treated BEAS-2B cells. (A,B) Western blot detection and quantitative analysis of E-cadherin and Claudin-1 protein expression in BEAS-2B cells. (C,D) Western blot detection and quantitative analysis of ferroptosis-related proteins (SLC7A11, FSP1, GPX4, TFR1) in BEAS-2B cells. N = 3, $^{\#}p < 0.05$ vs. Control group; $^{*}p < 0.05$ vs. IL-13 group.

SLC7A11, FSP1, GPX4) was evaluated by WB (Fig. 7G). IL-13 stimulation significantly decreased GSH levels and the expression of SLC7A11, FSP1, and GPX4, while significantly increasing iron content, MDA levels, and TFR1 expression ($p < 0.05$). Garcinol intervention significantly reversed these changes, elevating GSH, SLC7A11, FSP1, and GPX4 levels, and reducing iron content, MDA, and TFR1 levels ($p < 0.05$). This suggests that garcinol modulates ferroptosis and related proteins, thereby attenuating oxidative stress damage. Notably, the addition of EX527 abolished these protective effects, leading to significantly increased iron content, MDA, and TFR1 levels, and decreased GSH, SLC7A11, FSP1, and GPX4 levels ($p < 0.05$). This indicates that garcinol likely regulates ferroptosis by modulating the activity of ferroptosis-related proteins through the activation of the SIRT1/PPARα signaling pathway.

Finally, WB analysis of E-cadherin and Claudin-1 revealed that their expression was significantly downregulated by IL-13 stimulation ($p < 0.05$, Fig. 7H). Garcinol treatment significantly restored their expression ($p < 0.05$). However, this effect was attenuated by co-treatment with EX527, which showed decreased E-cadherin and Claudin-1 levels. This suggests that garcinol participates in regulating IL-13-induced airway epithelial barrier function, likely via the SIRT1/PPARα signaling pathway.

Discussion

Asthma, a prevalent chronic respiratory disease worldwide, remains a considerable clinical challenge due to persistently high incidence and disease burden. Although inhaled glucocorticoids are first-line therapies, their single anti-inflammatory mechanism limits clinical efficacy, with some patients exhibiting glucocorticoid insensitivity, resistance, or poor symptom control. The systemic side-effects of long-term treatment with high doses of inhaled glucocorticosteroids include easy bruising, adrenal suppression and decreased bone mineral density [27]. Therefore, the development of novel, efficacious drugs with diverse mechanisms of action remains an urgent need in asthma therapy.

Garcinol, a natural polyphenol derived from *Garcinia* species, has been reported to exhibit anti-inflammatory, antioxidant, anti-pulmonary fibrosis, immunoregulatory, and neuroprotective activities [14]. Its natural origin suggests relative safety; however, its specific role and mechanisms in asthma remain unclear. In this study, we established an OVA-induced murine asthma model to systematically evaluate garcinol's effects and mechanisms *in vivo* and applied an IL-13–stimulated BEAS-2B cell model *in vitro* to assess garcinol's therapeutic potential against allergic asthma. The results demonstrated that garcinol significantly atten-

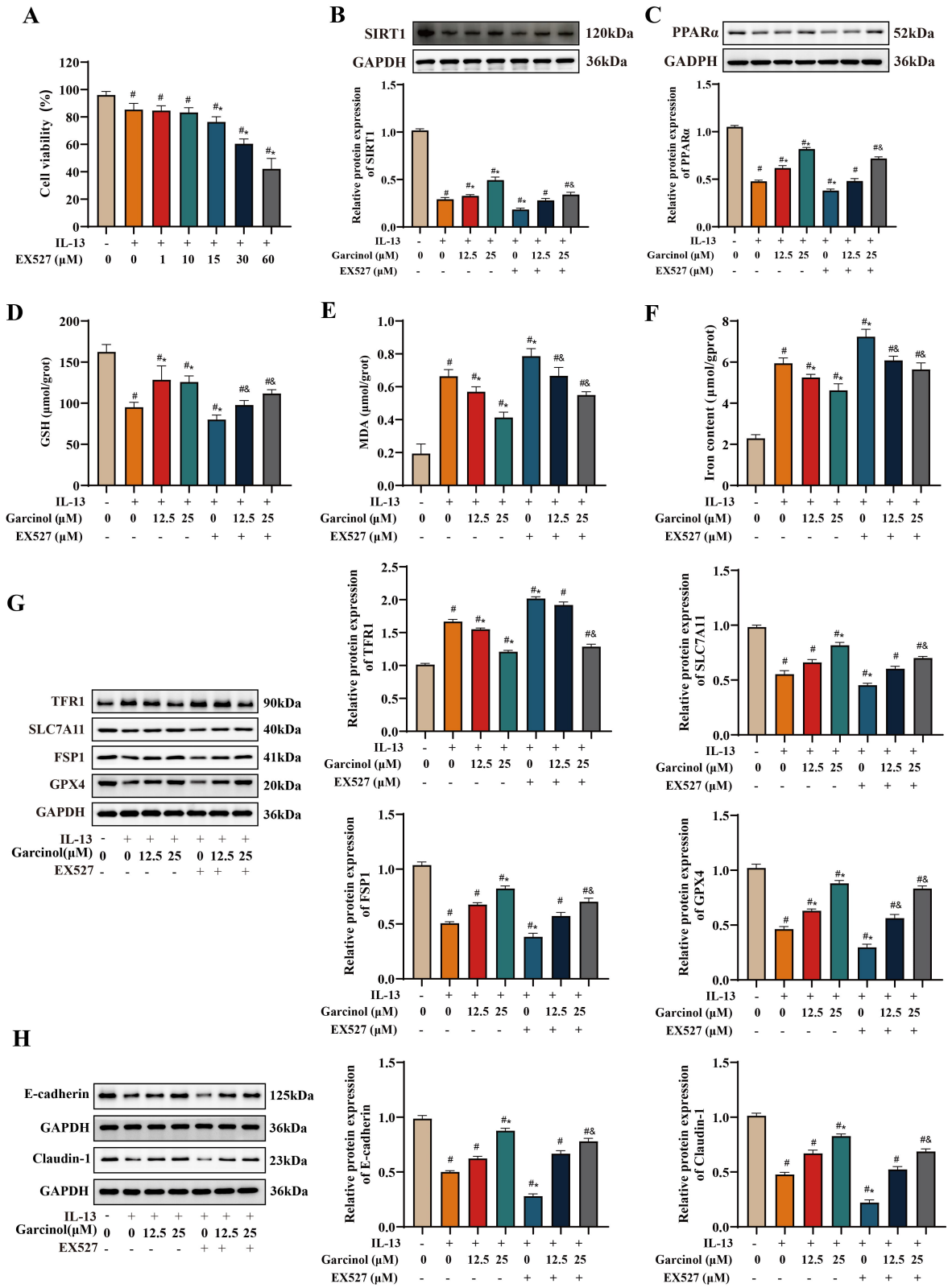

Fig. 7. Effects of garcinol on IL-13–treated BEAS-2B cells after SIRT1 inhibition by EX527. (A) Effects of different concentrations of EX527 on the viability of IL-13–treated BEAS-2B cells (n = 3). #, $p < 0.05$ vs. 0 ng; *, $p < 0.05$ vs. IL-13 group. (B,C) Western blot detection and quantitative analysis of SIRT1 (B) and PPARα (C) protein expression in each group. (D–F) Biochemical assays measuring GSH, MDA, and iron content in each group. (G) Western blot analysis of ferroptosis-related proteins (TFR1, SLC7A11, FSP1, GPX4) in each group. (H) Western blot analysis of E-cadherin and Claudin-1 protein expression in each group. N = 3, $^{\#}p < 0.05$ vs. CON group; $^{*}p < 0.05$ vs. IL-13 group; $^{\&}p < 0.05$ vs. the corresponding concentration of Garcinol group.

uated airway inflammation, inhibited airway remodeling, and modulated ferroptosis.

Garcinol Attenuates Airway Inflammation and Hyperresponsiveness in OVA-Induced Asthmatic Mice

Airway inflammation and hyperresponsiveness are core pathological features of asthma. Using OVA sensitization and challenge, we successfully established an allergic asthma model. Mice in the OVA group exhibited typical airway hyperresponsiveness, manifested by significantly increased airway resistance, elevated leukocytes, eosinophils, and neutrophils in BALF, and upregulated Th2 cytokines IL-4, IL-5, and IL-13. This phenotype is consistent with previous reports by Hayashi *et al.* [28], validating the reliability of our model.

Garcinol and budesonide intervention significantly reduced airway resistance, mitigated lung tissue damage, and suppressed BALF inflammatory cell infiltration and IL-4/IL-5/IL-13 release. Allergic asthma is primarily driven by Th2 immune responses, which, via IL-4, IL-5, and IL-13 secretion, mediate both acute asthma symptoms and airway remodeling [6,7]. The synergistic suppression of these key cytokines by garcinol suggests its potential to modulate critical nodes of Th2 immunity, alleviating acute inflammatory responses and providing experimental support for further drug development.

Garcinol Inhibits Airway Remodeling by Reducing Epithelial Inflammation and Restoring Barrier Function

Airway remodeling underlies chronic progression and irreversible pulmonary function decline in asthma. HE, PAS, and Masson staining revealed significant airway wall thickening, goblet cell hyperplasia, and collagen deposition in OVA mice, leading to luminal narrowing. Garcinol intervention markedly improved these structural abnormalities, indicating inhibition of airway remodeling and providing *in vivo* evidence of its role in asthma management.

Airway epithelium serves as a critical host-environment interface, maintaining tissue homeostasis. IL-13, a key asthma mediator, induces mucus hypersecretion and ciliary dysfunction, recapitulating clinical phenotypes [29]. IL-13 suppressed cell viability and promoted IL-6 and IL-1β release, which can further amplify inflammation in severe asthma [30]. Garcinol significantly reduced IL-6 and IL-1β in culture supernatants, consistent with its systemic anti-inflammatory effects in mice, indicating direct anti-inflammatory and protective effects on airway epithelium.

Furthermore, disruption of epithelial barrier integrity is a key factor facilitating allergen penetration and the persistence of chronic inflammation [10]. Claudin-1, a core tight junction protein, when downregulated, directly compromises airway epithelial barrier integrity, thereby exacerbating allergen infiltration and inflammatory responses [31]. E-cadherin, a major component of adherens junctions, can contribute to airway remodeling through intrinsic epithelial mechanisms and epithelial-immune signaling cascades when its expression is reduced [32]. In this study, we observed that the expression levels of both proteins were significantly decreased in the lung tissues of asthmatic mice and in IL-13-stimulated BEAS-2B cells, consistent with reports that Claudin-1 loss accelerates allergic responses [31] and E-cadherin downregulation promotes airway remodeling [32]. Garcinol treatment markedly upregulated the expression of these two proteins, providing molecular-level evidence for its ability to restore epithelial barrier function and inhibit airway remodeling, supporting its multi-targeted mechanism of action.

Critical Role of SIRT1/PPARα Signaling in Garcinol's Anti-Asthma Effects

Wu *et al.* [33] reported that morin alleviates sepsis-associated encephalopathy by inhibiting ferroptosis via SIRT1 activation. SIRT1 is a nicotinamide adenine dinucleotide (NAD+)-dependent deacetylase that modulates pulmonary immune/inflammatory responses and aging processes primarily through post-translational modifications, and it is implicated in the pathogenesis of various lung diseases, including asthma [34]. A recent study has shown that SIRT1 regulates the activity of steroid hormone receptors, interacts with glucocorticoid receptors, and plays a key role in glucocorticoid signaling [35]. In addition, SIRT1 regulates ferroptosis in multiple tissues, including the lungs [36,37]. Additionally, SIRT1 can modulate steroid receptor activity and interact with androgen receptor and glucocorticoid receptor (GR). In certain glucocorticoid-resistant diseases, reduced SIRT1 expression has been observed, suggesting that SIRT1 may represent a potential therapeutic target for pulmonary disorders and could provide novel opportunities for treating glucocorticoid-resistant asthma [34]. However, whether garcinol can regulate asthma by inhibiting ferroptosis via SIRT1 has not been reported.

PPARα, a member of the nuclear receptor superfamily, is a key downstream target of SIRT1 in lipid metabolism regulation and serves as an important transcriptional regulator in lipid transport and inflammatory processes [38]. A study has shown that PPARα agonists can improve ovalbumin-induced allergic asthma, although the precise mechanisms remain unclear [39]. Notably, PPARα and its mediated signaling pathways play a crucial role in the regulation of ferroptosis. On one hand, PPARα can activate antioxidant signaling pathways (such as Nrf2/ARE), indirectly upregulating SLC7A11 expression to enhance cystine uptake and GSH synthesis [40,41]; on the other hand, it can reduce iron-induced lipid peroxidation by inhibiting TFR1-mediated iron overload and regulating FSP1, thereby modulating ferroptosis [42,43]. To date, there are no reports

on whether garcinol can inhibit ferroptosis via PPARα or the SIRT1/PPARα axis to participate in asthma regulation.

Immunofluorescence and WB analyses showed that SIRT1 and PPARα expression in OVA mouse lungs was significantly reduced compared with CON, indicating their involvement in asthma pathology. Garcinol significantly increased SIRT1 and PPARα expression in the OVA+LG, OVA+HG, and OVA+BUD groups, representing *in vivo* evidence that garcinol may regulate asthma via SIRT1/PPARα modulation.

In IL-13–stimulated BEAS-2B cells, addition of SIRT1 inhibitor EX527 significantly reduced E-cadherin and Claudin-1 expression, similar to ferroptosis inhibition, consistent with Jiang *et al.* [34]. Garcinol restored these proteins, suggesting activation of SIRT1/PPARα mediates epithelial barrier protection, aligning with *in vivo* findings [35]. We innovatively suggest that garcinol may enhance glucocorticoid sensitivity via SIRT1/PPARα activation.

Garcinol Confers Pulmonary Protection by Modulating Ferroptosis

A recent study has shown that morin alleviates sepsis-associated encephalopathy by inhibiting ferroptosis through SIRT1 activation [33]. Ferroptosis contributes to the pathogenesis of asthma primarily through oxidative stress and dysregulated iron metabolism. Ferroptosis is regulated by several key signaling pathways. Particularly, depletion of GSH leads to GPX4 inactivation. The GPX4-GSH-system Xc^- axis constitutes the core execution mechanism of ferroptosis [44]. SLC7A11, also known as xCT, is a cystine transporter that not only contributes to GSH synthesis but also serves as a critical regulator of ferroptosis, with the GSH-GPX4 antioxidant axis mediating its ferroptosis-inhibitory function [45]. Transferrin receptor 1 and ferroptosis suppressor protein 1 are central regulators of ferroptosis, modulating the process through the disruption of iron homeostasis and lipid peroxidation pathways, respectively [46,47]. MDA, one of the end products of lipid peroxidation during ferroptosis, serves as an important indicator for assessing both lipid peroxidation levels and oxidative stress [46]. Our findings provide experimental and theoretical evidence supporting the therapeutic potential of garcinol in allergic asthma.

First, we observed classic hallmarks of ferroptosis in an OVA-induced asthmatic mouse model: tissue iron accumulation, elevated levels of lipid peroxidation products (MDA and ROS), and depletion of the key antioxidant GSH. At the molecular level, SLC7A11, GPX4, and FSP1 were downregulated, while the positive regulator TFR1 was upregulated in both lung tissue and injured BEAS-2B cells. SLC7A11 functions as a key element of the GSH-GPX4 antioxidant system, mediating cystine uptake required for GSH synthesis. GPX4, in turn, depends on GSH to detoxify lipid peroxides and serves as a pivotal regulator in preventing ferroptotic cell death. Downregulation of SLC7A11 and GPX4 signifies a collapse of the cellular antioxidant defense system [18,45]. FSP1, another major anti-ferroptotic protein independent of the GPX4 pathway, further exacerbates cellular sensitivity to oxidative stress when downregulated [48]. Conversely, upregulation of TFR1 promotes iron uptake, thereby catalyzing lipid peroxidation [49,50]. The increase in TUNEL-positive cells, although traditionally associated with apoptosis, can also result from the severe lipid peroxidation and ROS accumulation characteristic of ferroptosis, both of which can induce DNA damage. These findings provide evidence for the presence of active ferroptosis in lung tissue.

To further substantiate the role of ferroptosis in asthma-induced lung injury, IL-13-stimulated BEAS-2B cells were treated with Fer-1. Fer-1 treatment increased the levels of epithelial barrier proteins E-cadherin and Claudin-1 compared to the IL-13 group, confirming that inhibiting ferroptosis effectively alleviates asthma-associated airway epithelial damage. Furthermore, the IL-13+Fer-1 group showed significant upregulation of SLC7A11, FSP1, and GPX4 protein levels, alongside downregulation of TFR1. These findings indicate that ferroptosis inhibition effectively reduces IL-13-induced ferroptosis in BEAS-2B cells. These *in vitro* results are consistent with the animal findings, further supporting the pivotal role of ferroptosis in the initiation and progression of airway epithelial barrier injury.

The most critical finding of this study is that garcinol intervention reversed all the aforementioned ferroptosis-related alterations. Specifically, garcinol upregulated the expression of SLC7A11, GPX4, and FSP1, downregulated TFR1 expression, reduced MDA and ROS levels, and restored GSH content. These results suggest that inhibiting ferroptosis is a crucial upstream mechanism under which garcinol exerts its anti-inflammatory and epithelial protective effects. Excessive lipid peroxides and ROS generated during ferroptosis can directly damage cell membrane structures, trigger intense inflammatory responses, and disrupt the epithelial barrier. Therefore, garcinol likely exerts its beneficial effects on inflammation, barrier function, and airway remodeling by multi-target stabilization of iron metabolism and the antioxidant defense system, thereby inhibiting ferroptosis and oxidative stress. This aligns with the perspective proposed by Yin *et al.* [51], that targeting ferroptosis in lung epithelial cells represents a novel therapeutic strategy for asthma.

PPARα, a downstream factor of SIRT1, plays a significant role in lipid metabolism and inflammatory responses. Our data demonstrate that co-treatment with the SIRT1 inhibitor EX527 (IL-13+garcinol+EX527 group) abrogated the protective effects of garcinol. Specifically, it increased tissue iron accumulation, MDA, and ROS levels, depleted GSH content, downregulated SLC7A11, GPX4, and FSP1 expression, and upregulated TFR1 in BEAS-2B cells. This indicates that the SIRT1/PPARα pathway may regulate ferroptosis, potentially through modulating pathways such as

Nrf2/SLC7A11/GPX4 and FSP1, influencing not only airway epithelial injury but also the ferroptotic process. In summary, garcinol appears to play its important regulatory role across multiple pathological aspects of asthma by concurrently activating SIRT1 and PPARα, thereby modulating key ferroptosis-related proteins and mediating the ferroptosis process.

Conclusion

In summary, firstly, this study employed an asthmatic mouse model for *in vivo* experiments, demonstrating that garcinol intervention effectively attenuates airway inflammation, alleviates lung structural damage, and improves lung function, thereby significantly mitigating asthma-induced lung injury. Furthermore, garcinol appears to inhibit ferroptosis signaling, potentially via activation of the SIRT1/PPARα pathway. Secondly, using an IL-13-induced BEAS-2B cell injury model for *in vitro* studies, results consistent with the animal model were obtained, suggesting that garcinol's regulation of ferroptosis in these cells is dependent on the SIRT1/PPARα signaling pathway. Finally, intervention with the SIRT1 inhibitor EX527 in BEAS-2B cells further clarified that garcinol ameliorates IL-13-induced cell injury and alleviates asthma-related lung damage by inhibiting ferroptosis through the initiation of the SIRT1/PPARα signaling pathway.

To our knowledge, this study creatively reveals that garcinol exerts significant protective effects against asthma-induced lung injury by inhibiting ferroptosis via activation of the SIRT1/PPARα signaling pathway. In addition, garcinol also effectively suppresses airway inflammatory cytokines and attenuates airway epithelial damage, thereby helping to prevent asthma-related lung injury. Furthermore, garcinol may regulate steroid hormone receptor activity by activating the SIRT1 pathway, potentially offering a novel therapeutic strategy for patients with severe asthma.

Availability of Data and Materials

The data used and analyzed during the current study are available from the corresponding author.

Author Contributions

YLL and FFF contributed equally to the conception and design of the study. YLL was primarily responsible for data collection and analysis, as well as manuscript writing. FFF and YZZ jointly assisted in the interpretation of the research results and the writing of the manuscript. YLZ and BYX participated in data analysis and interpretation, and contributed to the drafting and revision of the manuscript. They also provided valuable feedback on the methodology and analysis of the study. QZ and BL were responsible for the overall project management and contributed to the study design and implementation. They also participated in the drafting and revision of the manuscript. All authors played significant roles in the advancement of the research and approved the final version of the manuscript. All authors have participated sufficiently in the work to take public responsibility for appropriate portions of the content and agreed to be accountable for all aspects of the work in ensuring that questions related to its accuracy or integrity are appropriately investigated and resolved.

Ethics Approval and Consent to Participate

This study was approved by the Experimental Animal Ethics Committee of the Third Affiliated Hospital of Zhengzhou University (Approval No. 2024-097-01). All procedures complied with the ARRIVE Guidelines 2.0.

Acknowledgment

Not applicable.

Funding

This research received no external funding.

Conflict of Interest

The authors declare no conflict of interest.

Supplementary Material

Supplementary material associated with this article can be found, in the online version, at https://doi.org/10.24976/Discov.Med.202638209.142.

References

[1] Global Initiative for Asthma. Global Strategy for Asthma Management and Prevention. 2024. Available at: https://ginasthma.org/2024-report/?utm_source=chatgpt.com (Accessed: 1 March 2026).

[2] Boulet LP. Airway remodeling in asthma: update on mechanisms and therapeutic approaches. Current Opinion in Pulmonary Medicine. 2018; 24: 56–62. https://doi.org/10.1097/MCP.0000000000000441.

[3] Holgate ST, Wenzel S, Postma DS, Weiss ST, Renz H, Sly PD. Asthma. Nature Reviews. Disease Primers. 2015; 1: 15025. https://doi.org/10.1038/nrdp.2015.25.

[4] Borkar NA, Ambhore NS, Balraj P, Ramakrishnan YS, Sathish V. Kisspeptin regulates airway hyperresponsiveness and remodeling in a mouse model of asthma. The Journal of Pathology. 2023; 260: 339–352. https://doi.org/10.1002/path.6086.

[5] Huang FL, Liao EC, Yu SJ. House dust mite allergy: Its innate immune response and immunotherapy. Immunobiology. 2018; 223: 300–302. https://doi.org/10.1016/j.imbio.2017.10.035.

[6] Abe Y, Suga Y, Fukushima K, Ohata H, Niitsu T, Nabeshima H, *et al*. Advances and Challenges of Antibody Therapeutics for Severe Bronchial Asthma. International Journal of Molecular Sciences. 2021; 23: 83. https://doi.org/10.3390/ijms23010083.

[7] Brasier AR. Therapeutic targets for inflammation-mediated air-

way remodeling in chronic lung disease. Expert Review of Respiratory Medicine. 2018; 12: 931–939. https://doi.org/10.1080/17476348.2018.1526677.

[8] Huang Y, Qiu C. Research advances in airway remodeling in asthma: a narrative review. Annals of Translational Medicine. 2022; 10: 1023. https://doi.org/10.21037/atm-22-2835.

[9] Shifren A, Witt C, Christie C, Castro M. Mechanisms of remodeling in asthmatic airways. Journal of Allergy. 2012; 2012: 316049. https://doi.org/10.1155/2012/316049.

[10] Russell RJ, Boulet LP, Brightling CE, Pavord ID, Porsbjerg C, Dorscheid D, *et al*. The airway epithelium: an orchestrator of inflammation, a key structural barrier and a therapeutic target in severe asthma. The European Respiratory Journal. 2024; 63: 2301397. https://doi.org/10.1183/13993003.01397-2023.

[11] Caramori G, Nucera F, Mumby S, Lo Bello F, Adcock IM. Corticosteroid resistance in asthma: Cellular and molecular mechanisms. Molecular Aspects of Medicine. 2022; 85: 100969. https://doi.org/10.1016/j.mam.2021.100969.

[12] Deb S, Phukan BC, Mazumder MK, Dutta A, Paul R, Bhattacharya P, *et al*. Garcinol, a multifaceted sword for the treatment of Parkinson's disease. Neurochemistry International. 2019; 128: 50–57. https://doi.org/10.1016/j.neuint.2019.04.004.

[13] Coste C, Gérard N, Dinh CP, Bruguière A, Rouger C, Leong ST, *et al*. Targeting MHC Regulation Using Polycyclic Polyprenylated Acylphloroglucinols Isolated from *Garcinia bancana*. Biomolecules. 2020; 10: 1266. https://doi.org/10.3390/biom10091266.

[14] Thoyajakshi RS, Megha GT, Ravi Kumar H, Mathad SN, Khan A, Nagaraju S, *et al*. Garcinol: A novel and potent inhibitor of hyaluronidase enzyme. International Journal of Biological Macromolecules. 2024; 266: 131145. https://doi.org/10.1016/j.ijbiomac.2024.131145.

[15] Kang Y, Sun Y, Li T, Ren Z. Garcinol protects against cerebral ischemia-reperfusion injury in vivo and in vitro by inhibiting inflammation and oxidative stress. Molecular and Cellular Probes. 2020; 54: 101672. https://doi.org/10.1016/j.mcp.2020.101672.

[16] Lee TK, Ashok Kumar K, Huang CY, Liao PH, Ho TJ, Kuo WW, *et al*. Garcinol protects SH-SY5Y cells against MPP+-induced cell death by activating DJ-1/SIRT1 and PGC-1α mediated antioxidant pathway in sequential stimulation of p-AMPK mediated autophagy. Environmental Toxicology. 2023; 38: 857–866. https://doi.org/10.1002/tox.23737.

[17] Cui ZL, Gu W, Ding T, Peng XH, Chen X, Luan CY, *et al*. Histone modifications of Notch1 promoter affect lung CD4+ T cell differentiation in asthmatic rats. International Journal of Immunopathology and Pharmacology. 2013; 26: 371–381. https://doi.org/10.1177/039463201302600210.

[18] Dixon SJ, Lemberg KM, Lamprecht MR, Skouta R, Zaitsev EM, Gleason CE, *et al*. Ferroptosis: an iron-dependent form of nonapoptotic cell death. Cell. 2012; 149: 1060–1072. https://doi.org/10.1016/j.cell.2012.03.042.

[19] Huang E, Wang X, Chen L. Regulated Cell Death in Endometriosis. Biomolecules. 2024; 14: 142. https://doi.org/10.3390/biom14020142.

[20] Liu X, Pan B, Wang X, Xu J, Wang X, Song Z, *et al*. Ischemia/reperfusion-activated ferroptosis in the early stage triggers excessive inflammation to aggregate lung injury in rats. Frontiers in Medicine. 2023; 10: 1181286. https://doi.org/10.3389/fmed.2023.1181286.

[21] Banerjee P, Balraj P, Ambhore NS, Wicher SA, Britt RD, Jr, Pabelick CM, *et al*. Network and co-expression analysis of airway smooth muscle cell transcriptome delineates potential gene signatures in asthma. Scientific Reports. 2021; 11: 14386. https://doi.org/10.1038/s41598-021-93845-x.

[22] Li X, Zhang J, Feng Y, Zhou Q, Zhang C. Modulation of the NF-κB signaling pathway by the combined strategy of tocilizumab and dexamethasone for asthma therapy. Respiratory Research. 2026; 27: 44. https://doi.org/10.1186/s12931-025-03458-5.

[23] Zou J, Chen H, Fan X, Qiu Z, Zhang J, Sun J. Garcinol prevents oxidative stress-induced bone loss and dysfunction of BMSCs through NRF2-antioxidant signaling. Cell Death Discovery. 2024; 10: 82. https://doi.org/10.1038/s41420-024-01855-1.

[24] Sun Y, Wang J, Li H, Sun L, Wang Y, Han X. The effects of budesonide on angiogenesis in a murine asthma model. Archives of Medical Science: AMS. 2013; 9: 361–367. https://doi.org/10.5114/aoms.2013.33194.

[25] Liu P, Feng Y, Li H, Chen X, Wang G, Xu S, *et al*. Ferrostatin-1 alleviates lipopolysaccharide-induced acute lung injury via inhibiting ferroptosis. Cellular & Molecular Biology Letters. 2020; 25: 10. https://doi.org/10.1186/s11658-020-00205-0.

[26] Lei Y, Zhu Y, Mallah MA, Lu P, Yang L, He X, *et al*. The activation of SIRT1 ameliorates BPDE-induced inflammatory damage in BEAS-2B cells via HMGB1/TLR4/NF-κB pathway. Environmental Toxicology. 2023; 38: 2429–2439. https://doi.org/10.1002/tox.23878.

[27] Bateman ED, Hurd SS, Barnes PJ, Bousquet J, Drazen JM, FitzGerald JM, *et al*. Global strategy for asthma management and prevention: GINA executive summary. European Respiratory Journal. 2008; 31: 143–178. https://doi.org/10.1183/09031936.00138707.

[28] Hayashi T, Adachi Y, Hasegawa K, Morimoto M. Less sensitivity for late airway inflammation in males than females in BALB/c mice. Scandinavian Journal of Immunology. 2003; 57: 562–567. https://doi.org/10.1046/j.1365-3083.2003.01269.x.

[29] Malavia NK, Mih JD, Raub CB, Dinh BT, George SC. IL-13 induces a bronchial epithelial phenotype that is profibrotic. Respiratory Research. 2008; 9: 27. https://doi.org/10.1186/1465-9921-9-27.

[30] Pham DD, Kim TB. Epithelial-derived cytokines in the pathogenesis of severe asthma. Frontiers in Allergy. 2025; 6: 1681147. https://doi.org/10.3389/falgy.2025.1681147.

[31] Xia Y, Cao H, Zheng J, Chen L. Claudin-1 Mediated Tight Junction Dysfunction as a Contributor to Atopic March. Frontiers in Immunology. 2022; 13: 927465. https://doi.org/10.3389/fimmu.2022.927465.

[32] Young RE, Lee S, Chin J, Dash B, Sahi J, Nantie LB, *et al*. Disruption of E-cadherin in the airway led to dysplastic stressed cells and asthma-like phenotypes. Developmental Cell. 2025; 60: 3050–3065.e5. https://doi.org/10.1016/j.devcel.2025.06.030.

[33] Wu Z, Li H, Zhang X, Yang Y, Hu W, Hu B, *et al*. Morin alleviates sepsis-associated encephalopathy through inhibiting ferroptosis via SIRT1. Brain Research Bulletin. 2025; 233: 111638. https://doi.org/10.1016/j.brainresbull.2025.111638.

[34] Jiang YZ, Huang XR, Chang J, Zhou Y, Huang XT. SIRT1: An Intermediator of Key Pathways Regulating Pulmonary Diseases. Laboratory Investigation. 2024; 104: 102044. https://doi.org/10.1016/j.labinv.2024.102044.

[35] Xie J, Che S, Liu J, Long X. SIRT1: potential target in glucocorticoid-resistant diseases. Frontiers in Immunology. 2025; 16: 1514745. https://doi.org/10.3389/fimmu.2025.1514745.

[36] Zeng J, Guo J, Huang S, Cheng Y, Luo F, Xu X, *et al*. The roles of sirtuins in ferroptosis. Frontiers in Physiology. 2023; 14: 1131201. https://doi.org/10.3389/fphys.2023.1131201.

[37] Yang K, Dong W. SIRT1-Related Signaling Pathways and Their Association With Bronchopulmonary Dysplasia. Frontiers in Medicine. 2021; 8: 595634. https://doi.org/10.3389/fmed.2021.595634.

[38] Wu D, Yang Y, Hou Y, Zhao Z, Liang N, Yuan P, *et al*. Increased mitochondrial fission drives the reprogramming of fatty

acid metabolism in hepatocellular carcinoma cells through suppression of Sirtuin 1. Cancer Communications. 2022; 42: 37–55. https://doi.org/10.1002/cac2.12247.

[39] Lee YE, Im DS. Elafibranor PPARα/δ Dual Agonist Ameliorates Ovalbumin-Induced Allergic Asthma. Biomolecules & Therapeutics. 2024; 32: 460–466. https://doi.org/10.4062/biomolther.2023.194.

[40] Feng Y, Wang H, Hu Y, Zhang X, Miao X, Li Z, *et al*. Hederagenin ameliorates ferroptosis-induced damage by regulating PPARα/Nrf2/GPX4 signaling pathway in HT22 cells: An in vitro and in silico study. Bioorganic Chemistry. 2025; 155: 108119. https://doi.org/10.1016/j.bioorg.2024.108119.

[41] Wang H, Wu S, Jiang X, Li W, Li Q, Sun H, *et al*. Acteoside alleviates salsolinol-induced Parkinson's disease by inhibiting ferroptosis via activating Nrf2/SLC7A11/GPX4 pathway. Experimental Neurology. 2025; 385: 115084. https://doi.org/10.1016/j.expneurol.2024.115084.

[42] Liu Y, Ni F, Huang J, Hu Y, Wang J, Wang X, *et al*. PPAR-α inhibits DHEA-induced ferroptosis in granulosa cells through upregulation of FADS2. Biochemical and Biophysical Research Communications. 2024; 715: 150005. https://doi.org/10.1016/j.bbrc.2024.150005.

[43] Guo J, Le Y, Yuan A, Liu J, Chen H, Qiu J, *et al*. Astragaloside IV ameliorates cisplatin-induced liver injury by modulating ferroptosis-dependent pathways. Journal of Ethnopharmacology. 2024; 328: 118080. https://doi.org/10.1016/j.jep.2024.118080.

[44] Jiang C, Yan Y, Long T, Xu J, Chang C, Kang M, *et al*. Ferroptosis: a potential therapeutic target in cardio-cerebrovascular diseases. Molecular and Cellular Biochemistry. 2025; 480: 4379–4399. https://doi.org/10.1007/s11010-025-05262-7.

[45] Qiu H, Liu J, Shao N, Zhao J, Chen C, Jiang Y, *et al*. SLC7A11 as a bridge between ferroptosis and disulfidptosis: a promising target for tumor treatment. Cell Communication and Signaling: CCS. 2025; 23: 460. https://doi.org/10.1186/s12964-025-02447-x.

[46] Khatun J, Gelles JD, Chipuk JE. Dynamic death decisions: How mitochondrial dynamics shape cellular commitment to apoptosis and ferroptosis. Developmental Cell. 2024; 59: 2549–2565. https://doi.org/10.1016/j.devcel.2024.09.004.

[47] Koppula P, Lei G, Zhang Y, Yan Y, Mao C, Kondiparthi L, *et al*. A targetable CoQ-FSP1 axis drives ferroptosis- and radiation-resistance in KEAP1 inactive lung cancers. Nature Communications. 2022; 13: 2206. https://doi.org/10.1038/s41467-022-29905-1.

[48] Emmanuel N, Li H, Chen J, Zhang Y. *FSP1*, a novel KEAP1/NRF2 target gene regulating ferroptosis and radioresistance in lung cancers. Oncotarget. 2022; 13: 1136–1139. https://doi.org/10.18632/oncotarget.28301.

[49] Kawabata H. Transferrin and transferrin receptors update. Free Radical Biology & Medicine. 2019; 133: 46–54. https://doi.org/10.1016/j.freeradbiomed.2018.06.037.

[50] An Q, Wei R, Huang Z, Tang Y, Wang M, He S, *et al*. Palmitoylation of Tfr1 enhances platelet ferroptosis and liver injury in heat stroke. Acta Pharmaceutica Sinica. B. 2026; 16: 270–286. https://doi.org/10.1016/j.apsb.2025.10.027.

[51] Yin X, Hou X, Feng J. Role of Ferroptosis on Lung Epithelial Cells in Disease Progression and Treatment: A Review. Medical Science Monitor: International Medical Journal of Experimental and Clinical Research. 2025; 31: e948226. https://doi.org/10.12659/MSM.948226.